arXiv:1406.7834v2 [astro-ph.HE] 27 Oct 2014

Electrodynamics of axisymmetric pulsar magnetosphere with electron-positron discharge: a numerical experiment

Alexander Y. Chen, Andrei M. Beloborodov

Physics Department and Columbia Astrophysics Laboratory, Columbia University, 538 West 120th Street New York, NY 10027

ABSTRACT

We present the first self-consistent global simulations of pulsar magnetospheres with operating $e^{\pm}$ discharge. We focus on the simple configuration of an aligned or anti-aligned rotator. The star is spun up from zero (vacuum) state to a high angular velocity, and we follow the coupled evolution of its external electromagnetic field and plasma particles using the "particle-in-cell" method. A plasma magnetosphere begins to form through the extraction of particles from the star; these particles are accelerated by the rotation-induced electric field, producing curvature radiation and igniting $e^{\pm}$ discharge. We follow the system evolution for several revolution periods, longer than required to reach a quasi-steady state. Our numerical experiment puts to test previous ideas for the plasma flow and gaps in the pulsar magnetosphere.

We first consider rotators capable of producing pairs out to the light cylinder through photon-photon collisions. We find that their magnetospheres are similar to the previously obtained force-free solutions with a Y-shaped current sheet. The magnetosphere continually ejects $e^{\pm}$ pairs and ions. Pair creation is sustained by a strong electric field along the current sheet. We observe powerful curvature and synchrotron emission from the current sheet, consistent with *Fermi* observations of gamma-ray pulsars.

We then study pulsars that can only create pairs in the strong-field region near the neutron star, well inside the light cylinder. We find that both aligned and anti-aligned rotators relax to the "dead" state with suppressed pair creation and electric currents, regardless of the discharge voltage.

Subject headings: acceleration of particles — magnetic fields — plasmas — radiation mechanisms: nonthermal — pulsars: general — gamma rays: theory

1. Introduction

The standard picture of pulsar magnetosphere assumes that it is filled with plasma and corotates with the neutron star with angular velocity Ω (Goldreich & Julian 1969, hereafter GJ). GJ considered the aligned rotator (magnetic dipole moment $\boldsymbol{\mu}$ parallel to $\boldsymbol{\Omega}$); then it was generalized to inclined rotators. The plasma sustains the "corotational" electric field $\mathbf{E} \approx -\mathbf{v}_{\rm rot} \times \mathbf{B}/c$ (with $\mathbf{v}_{\rm rot} = \boldsymbol{\Omega} \times \mathbf{r}$), which implies the local charge density $4\pi\rho_{\rm GJ} = \nabla\cdot\mathbf{E} \approx -2\boldsymbol{\Omega}\cdot\mathbf{B}/c$. A key feature of the GJ model is the electric current $I_{\rm GJ}$ flowing out of and into the star along the open magnetic field lines that extend to the light cylinder $R_{\rm LC} = c/\Omega$. GJ showed that the open field lines are twisted and exert a spindown torque on the rotator. The circulating current is $I_{\rm GJ} \approx \mu\Omega^2/c$, and the corresponding spindown power is $\dot{E} \approx \Omega^4\mu^2/c^3$.

This picture was, however, never verified by a first-principle calculation and was questioned (Michel 2004; Gruzinov 2013). It was shown that charges lifted from the star by the rotation-induced electric field form the "electrosphere" — a corotating dome+torus structure, with a huge gap between them and no electric current (Jackson 1976; Krause-Polstorff & Michel 1985). Although the electrosphere is prone to diocotron instability (Pétri et al. 2002; Spitkovsky & Arons 2002), it was unclear if it could relax to the GJ state.

In addition to lifted charges, $e^{\pm}$ pairs are created around pulsars (Sturrock 1971). This provides plasma capable of screening the electric field component parallel to the magnetic field, $E_\parallel$. The negligible plasma inertia and $E_\parallel = 0$ provide the "force-free" (FF) conditions, which imply GJ corotation. The global solution for FF magnetospheres was obtained using various numerical techniques (Contopoulos et al. 1999; Timokhin 2006; Spitkovsky 2006; Kalapotharakos & Contopoulos 2009; Parfrey et al. 2012). Its characteristic feature is a thin current sheet supporting a discontinuity of $\mathbf{B}$ and the Y-point near the light cylinder. It was verified with particle-in-cell (PIC) simulations that sprinkling pairs with a high rate everywhere around the neutron star would drive the magnetosphere to the FF configuration (Philippov & Spitkovsky 2014).

A self-consistent model must, however, demonstrate how and where the plasma is created and to identify the regions of $E_\parallel \neq 0$ (called "gaps") where particles are accelerated to high energies. Besides testing the FF approximation, the self-consistent model would show how the pulsar radiation is produced, how the plasma flows in the magnetosphere and gets ejected. This problem was posed soon after the discovery of pulsars and proved to be difficult. Three types of gaps were proposed: polar-cap gap (Sturrock 1971; Ruderman & Sutherland 1975), slot gap (Arons 1983; Muslimov & Harding 2004), and outer gap (Cheng et al. 1986).

The only reliable way to solve the problem is a first-principle calculation of the self-

consistent dynamics of the electromagnetic field and pair discharge in the magnetosphere. Below we present such a direct numerical experiment. Our simulations are performed with a new 2.5D PIC code, developed from scratch and designed for neutron-star magnetospheres. The code calculates the fully relativistic dynamics of particles and fields on a curvilinear grid, traces the emission of gamma-rays and their conversion to pairs. The fields obey Maxwell equations, $\partial \mathbf{B}/\partial t = -c\nabla \times \mathbf{E}$ and $\partial \mathbf{E}/\partial t = c\nabla \times \mathbf{B} - 4\pi \mathbf{J}$, and exert force on particles $e(\mathbf{E} + \mathbf{v} \times \mathbf{B}/c)$. We use Esirkepov (2001) charge-conserving scheme for calculating $\mathbf{J}$ and a semi-implicit algorithm for the field evolution. A detailed description of the code and tests are given in the accompanying paper (Chen & Beloborodov, in preparation).

Pair creation by accelerated particles occurs in two steps: production of gamma-rays and their conversion to $e^{\pm}$. In many pulsars, the conversion is only efficient at $r \ll R_{\rm LC}$ where the magnetic field is strong. In young fast pulsars pairs can be created through photon-photon collisions inside and around the light cylinder (Cheng et al. 1986). For brevity, we call such rotators "type I." Pulsars with pair creation confined to $r \ll R_{\rm LC}$ will be called type II.

2. Problem formulation and simulation setup

The axisymmetric pulsar is described by its radius $R_\star \approx 10$ km, angular velocity $\mathbf{\Omega}$, and magnetic dipole moment $\boldsymbol{\mu}$ (aligned or anti-aligned with $\mathbf{\Omega}$). These parameters set the energy scale of the problem. The neutron star is a nearly ideal conductor, and its rotation induces voltage $\Phi_0 \approx \mu\Omega^2/c^2$ across the footprint of the open field line bundle; it corresponds to possible particle acceleration up to Lorentz factors $\gamma_0 = e\Phi_0/m_e c^2$. We start our simulations with $\Omega = 0$ and the vacuum dipole field. Then we gradually spin up the star: Ω grows linearly until it reaches its final value at $t_0 = 10R_\star/c$; $\Omega = const$ afterwards.

Corotational charge density $\rho_{\rm GJ} \approx -\mathbf{\Omega}\cdot\mathbf{B}/2\pi c$ defines the characteristic particle density $n = |\rho_{\rm GJ}|/e$, plasma frequency $\omega_p = (4\pi n e^2/m_e)^{1/2}$, and skin-depth $\lambda_p = c/\omega_p$. The magnetic field also determines the gyro-frequency of $e^{\pm}$, $\omega_B = eB/m_e c$, and ions, $\omega_{B,i} = eB/m_i c$. In a dipole magnetic field the characteristic frequencies are related by $\omega_p^2 = 2\omega_B\Omega$ and satisfy $\Omega \ll \omega_p \ll \omega_B$. The particle Larmor radius satisfies $r_{\rm L} \ll r$ at $r \ll R_{\rm LC}$, so particles move nearly along $\mathbf{B}$. At the light cylinder, $r_{\rm L} \sim (\gamma/\gamma_0)R_{\rm LC}$ may become comparable to $R_{\rm LC}$.

The characteristic λ_p at the polar cap is related to particle acceleration, as $\gamma_0 \approx (1/4)(R_\star/R_{\rm LC})(R_\star/\lambda_p)^2$. Typical pulsars have $R_\star/\lambda_p \sim 10^6 \gg 1$ and $R_{\rm LC}/R_\star \sim 10^2 - 10^3$. We scale down the big numbers, preserving the hierarchy of scales. The scale λ_p must be well resolved in the simulation, and the number of particles per grid cell must be large. This can only be achieved by increasing $\lambda_p/R_\star$. The simulations presented below have

$R_\star/\lambda_p \approx 100 - 130$, $R_{\rm LC}/R_\star = 6 - 10$, and $\gamma_0 = 425$. We also reduced the ion mass, $m_i = 5m_e$, and assumed ion charge number $Z = 1$.

We use spherical coordinates r, θ, ϕ, and our grid is uniformly spaced in $\log r$ and θ to allow better resolution near the star, where it is most needed. The grid size is 512×512.

Three field components are continuous at the star surface which defines the boundary conditions: $B_r = 2\mu \cos\theta/R_\star^3$, $E_\theta = -\mu\Omega \sin 2\theta/R_\star^2$, and $E_\phi = 0$. The dipole configuration of the magnetosphere is set by the surface B_r, and its rotation is communicated from the star through the surface E_θ. The star is also a source of electrons and ions for the magnetosphere. We make both particle species available below the surface and their extraction is self-consistently controlled by the local electric field. We neglect the work function, so that particles are easily lifted from the star.

The outer boundary is set at $R_{\rm out} = 30R_\star \gg R_{\rm LC}$. Here we place a "damping layer" of thickness $\Delta R = R_{\rm out}/15$. The layer has resistivity and damps electromagnetic fields on a timescale $\sim \Delta R/c$. Particles escape freely; they are decoupled from the fields once they enter the damping layer. With this implementation, the boundary effectively absorbs waves and particles, which is equivalent to their free escape.

Once an electron or positron reaches the threshold energy $\gamma_{\rm thr} m_e c^2$ it begins to emit curvature photons capable of pair creation. It depends on the curvature radius of the particle trajectory R_c as $\gamma_{\rm thr} = K(R_c/R_\star)^{1/3}$. In real pulsars $K \gtrsim 10^6$; we scale it down to $K = 20$ to allow copious pair creation in our numerical experiment. The photon emission rate is $\dot{N} = 0.25c(\gamma/R_c)$, where γ is the particle Lorentz factor. The photon emission, propagation, and conversion are traced using Monte-Carlo technique. The free paths of photons l have a distribution $P(l)$ with mean value $\bar{l}$ and dispersion Δl. The extreme case of $\bar{l} = 0$ is only relevant for discharge near magnetars (Beloborodov & Thompson 2007); for ordinary pulsars, the delay l/c should be included. In our simulations $\bar{l} = \Delta l = 2R_\star$ for photon-photon collisions (operating in rotators of type I) and $\bar{l} = \Delta l = 0.2R_\star$ for magnetic conversion (enabled at $r \lesssim 3R_\star$). The emitted photons have energies $E_{\rm ph} \ll \gamma_{\rm thr} m_e c^2$, and hence the secondary pairs are created with Lorentz factors $\gamma_s \ll \gamma_{\rm thr}$. The condition $\gamma_s \ll \gamma_{\rm thr} \ll \gamma_0$ ensures sufficient pair supply in the magnetosphere, and is satisfied in our simulations. Radiation reaction (energy loss due to gamma-ray emission) is explicitly included in the particle dynamics.

Hereafter distance is measured in $R_\star$, time in $R_\star/c$, energy in $m_e c^2$, magnetic and electric fields in $m_e c^2/eR_\star$, and charge density in $m_e c^2/4\pi e R_\star^2$.

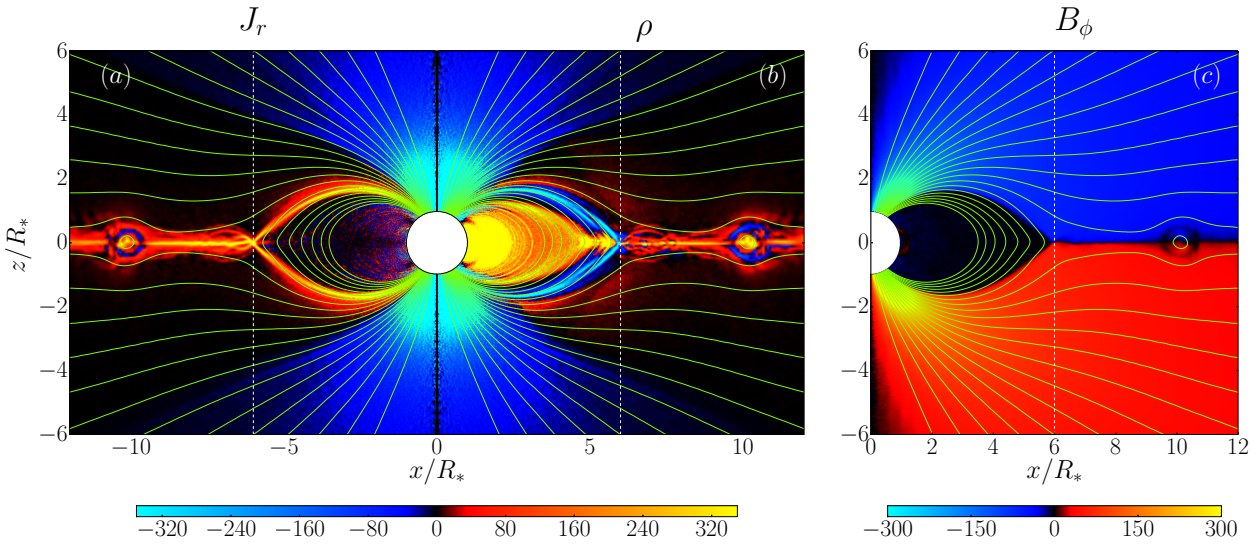

Fig. 1.— Magnetosphere of type I aligned rotator (poloidal cross section) at $t = 100$. Vertical dashed line shows the light cylinder. Green curves show the magnetic flux surfaces. (a) Radial component of electric current density J_r. (b) Net charge density ρ. (c) Toroidal component of the magnetic field B_ϕ.

3. Rotators of type I

Figures 1–3 show the magnetosphere of the aligned rotator with $R_{\rm LC} = 6$ and $\mu = 1.5 \times 10^4$ after 2.6 rotation periods. The energy density is almost everywhere dominated by the electromagnetic field, and the discharge finds a way to adjust and supply the charge density and electric currents demanded by the field. As a result, the magnetosphere shares several key features with the FF solution. Electric currents and Poynting flux flow through the light cylinder along the open magnetic field lines while the interior of the closed field-line zone has $\mathbf{J} = 0$ and $B_\phi = 0$. The Y-point is observed near $R_{\rm LC}$.

There are two distinct regions of negative and positive radial current density J_r. The negative current flows in the polar region around the magnetic axis. The positive current is concentrated in a current sheet supporting the jump of B_ϕ between the closed and open zones. Outside the light cylinder, the current sheet extends along the equatorial plane to support the flip of B_ϕ and B_r across the equatorial plane.

Charge density $\rho = \nabla \cdot \mathbf{E}/4\pi$ also conforms to the expectations from the FF model (cf. Figure 16 in Parfrey et al. 2012). In particular, the current sheet is positively charged outside the Y-point and negatively charged inside the Y-point (see Timokhin 2006 for discussion). ρ significantly deviates from the FF model in the neutral black region with $J_r = 0$; if the rotator

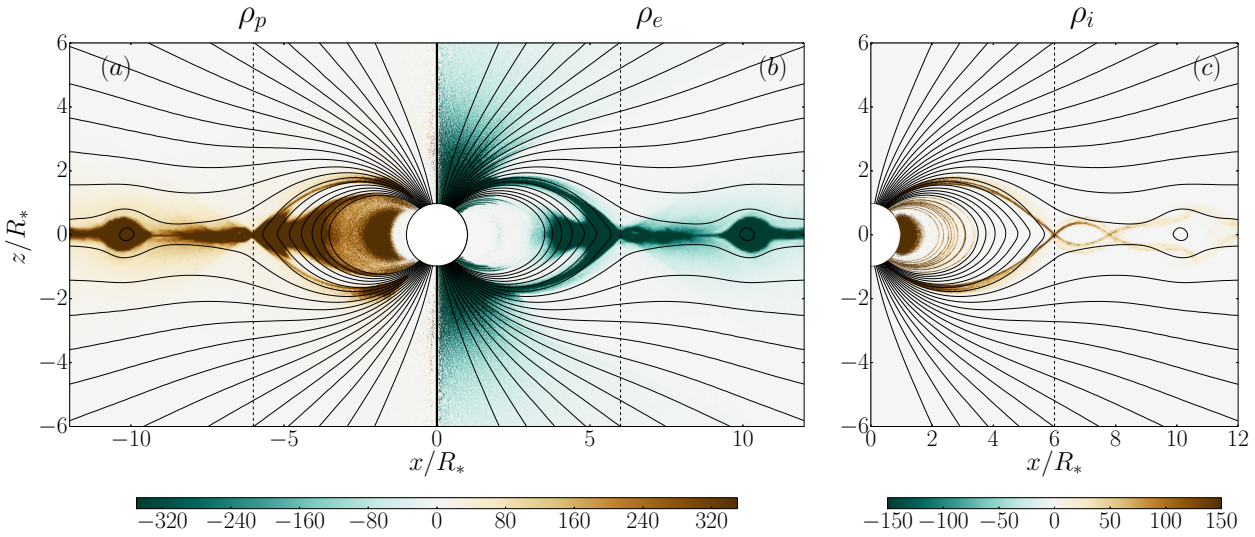

Fig. 2.— Charge densities of (a) positrons, (b) electrons, and (c) ions.

approaches the "death line" for pair creation, $\gamma_{\rm thr} \sim \gamma_0$, this region grows and occupies most of the magnetosphere. A similar neutral region was described by Yuki & Shibata (2012).

The two opposite currents are sustained by different mechanisms. The negative current in the polar region is carried by electrons lifted from the polar cap. There is no significant activity in this region; the particle acceleration is weak and pair creation does not occur. The absence of polar-cap activity is explained by the low positive value of $\alpha \equiv J_\parallel/c\rho_{\rm GJ} \sim 0.7 < 1$. It leads to easy screening of $E_\parallel$ by the charge-separated flow extracted from the star and the flow Lorentz factor comparable to $2\alpha/(1-\alpha^2)$ (Beloborodov 2008; Chen & Beloborodov 2013). We observed the same behavior in the simulation of anti-aligned rotator where currents switch sign and the polar current is carried by ions extracted from the star.

The opposite current (the current sheet) is sustained by $e^\pm$ discharge at $r < R_{\rm LC}$. It cannot be conducted by particles lifted from the star as its sign is opposite to that of the charge density demanded by the magnetosphere. Note also that $|\rho| \gg |\rho_{\rm GJ}|$ in the current sheet, so $\rho_{\rm GJ}$ is not important. The accelerating potential drop is $\Phi_\parallel \sim 2\pi\rho\delta^2 \sim -(\delta/r)\Phi_0$ where δ is the sheet thickness and we used $2\pi r\delta|\rho|c \sim I_{\rm GJ} = c\Phi_0$. Pair creation is biased to the outer side of the sheet (a result of its curvature and the finite free path of photons), therefore the unscreened $\Phi_\parallel$ is largest on the inner side. The sheet thickness δ is set by the Larmor radius of particles near the Y-point.

Plasma outflows along the equatorial plane outside $R_{\rm LC}$ and the Y-point resembles a nozzle formed by the open magnetic fluxes of opposite polarity. Two plasma streams come to

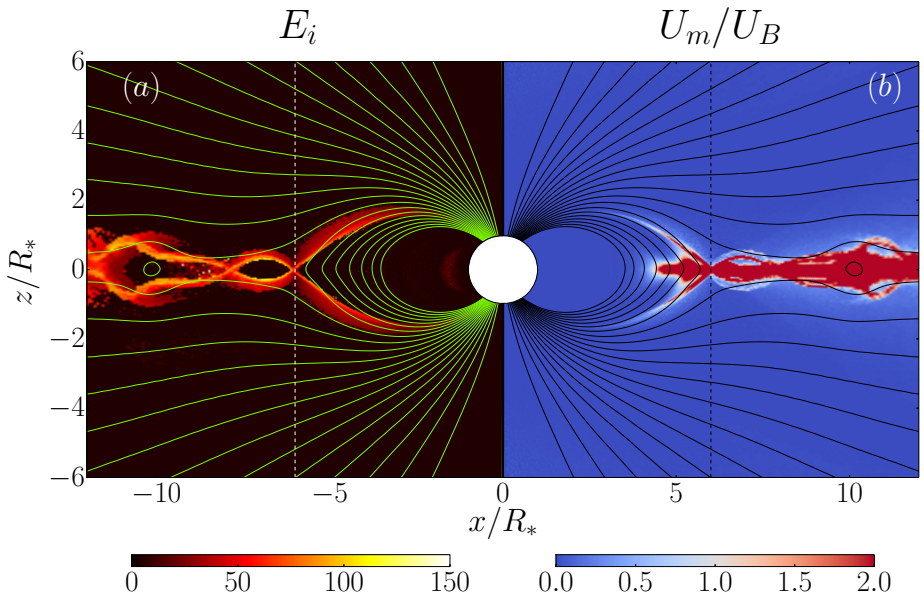

Fig. 3.— (a) Average ion energy in units of $m_e c^2$. (b) Ratio of total matter energy density U_m to magnetic energy density $U_B = B^2/8\pi$.

the Y-point along the boundary of the closed zone and exchange their opposite θ-momenta. Their collimation is achieved through gyration in the (predominantly toroidal) magnetic field, which communicates the θ-momentum from one stream to the other. As a result the streams flow out in the direction of their net momentum, which is radial (see also Shibata 1985).

About 10% of current is carried by the ions extracted from the star at the footpoints of the current sheet. Ions experience no radiative losses and tap the full $\Phi_\parallel$ (Figure 3a). They have the largest Larmor radius $r_{\rm L}$, so the ion streams show large oscillations around the equatorial plane (Figure 2c). The streams with smaller oscillations are formed by accelerated positrons with γ limited by radiation reaction. Secondary particles have even smaller energies; they outflow almost exactly in the equatorial plane. The streams with different $r_{\rm L}$ contribute to the thickening of the equatorial current sheet as seen in Figures 1-3.

Since ions do not create pairs, the discharge in the current sheet relies on the accelerated $e^\pm$. This requires continual recycling of created particles as seeds for new rounds of pair creation, which leads to voltage oscillations. The oscillations occur on the timescale $\sim R_{\rm LC}/c = \Omega^{-1}$ and make the magnetosphere "breath" around $R_{\rm LC}$.

There is a steep potential drop across the outer closed field lines toward the Y-point. The strong E_r helps eject particles into the equatorial current sheet. In this region $E \approx B$

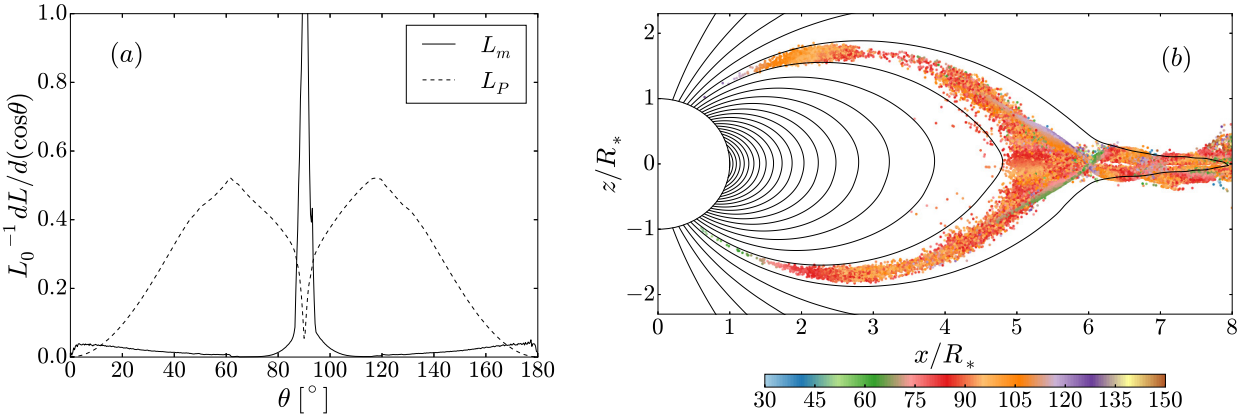

Fig. 4.— (a) Angular distribution of Poynting flux L_P and kinetic energy flux L_m at radius $2R_{\rm LC}$, normalized to $L_0 = \mu^2\Omega^4/c^3$. (b) Locations of gamma-ray emission events. Color shows the angle of the photon direction with respect to $\hat{\mathbf{z}}$.

and the particle ejection across $\mathbf{B}$ is assisted by the drop of B near the Y-point on a scale $\sim r_{\rm L}$.

The magnetic field dominates energy density everywhere except the Y-point region and the matter-dominated equatorial outflow (Figure 3b). This behavior is also visible in the angular distributions of the Poynting luminosity L_P and matter kinetic power L_m (Figure 4a). The integrated luminosities at $r = 2R_{\rm LC}$ are $L_P \approx 0.7L_0$ and $L_m \approx 0.15L_0$ where $L_0 = \mu^2\Omega^4/c^3$. Both contribute to the energy flux from the rotator. This should be compared with the spindown power extracted from the star, $L_{\rm sd} = L_P(R_\star) \approx 0.88L_0$. The difference between $L_{\rm sd}$ and $L_P + L_m$ is carried by particles bombarding the star (the backflow power is $\sim 0.1L_m$) and the gamma-rays.

At $r \gg R_{\rm LC}$ we observe magnetic reconnection which strongly heats particles in the equatorial outflow, forms large plasmoids, kinks and wiggles. They are advected outward and do not affect the current structure near the Y-point.

The current sheet is the only source of gamma-rays (Figure 4b). The emission is strongly anisotropic, peaking at $\pm \sim 12^\circ$ around the equatorial plane. In addition, there is a strong peak at the equator from the high-energy particles gyrating in the equatorial outflow.

The simulation for the anti-aligned rotator shows a similar magnetosphere but somewhat different discharge. The current sheet extracts and accelerates electrons from the star (instead of ions), which helps produce pairs. This leads to a more stable $\Phi_\parallel$ and reduces the "breathing" of the magnetosphere, so the Y-point is nearly static.

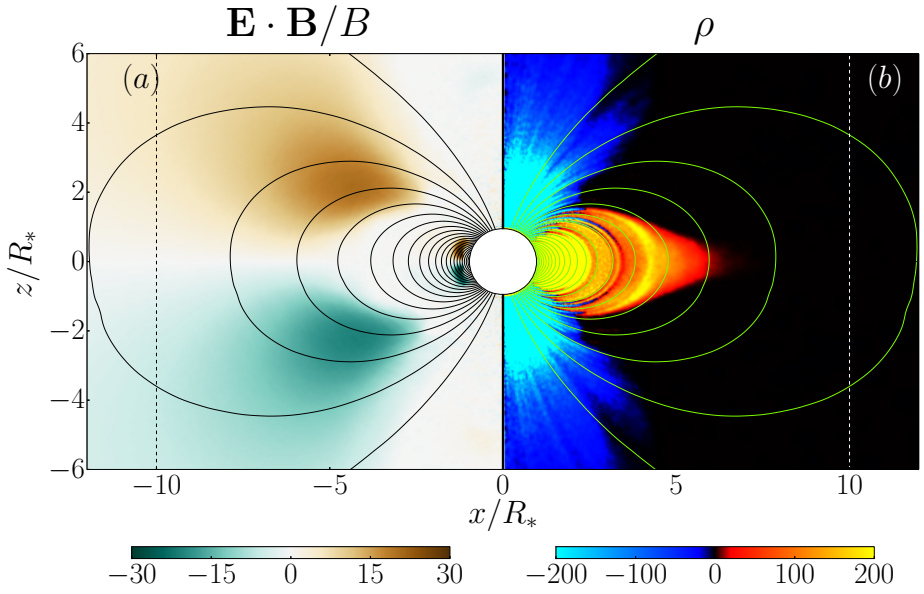

Fig. 5.— Type II magnetosphere at $t = 280$. (a) Parallel electric field $E_\parallel$. (b) Charge density ρ.

We also performed runs for the aligned and anti-aligned rotators with different rotation rates, magnetic fields, and $\gamma_{\rm thr}$. The exact position of the Y-point R_Y depends on these parameters. With extremely low $\gamma_{\rm thr}$ and copious supply of plasma R_Y decreases. If $\gamma_{\rm thr}/\gamma_0$ is increased to ~ 1, the magnetosphere transitions to the electrosphere state.

4. Rotators of type II

The simulation of type II rotators is the same as for type I except for three changes: we suppressed pair creation where $B < 400$, which roughly corresponds to $r \gtrsim 4$, increased $R_{\rm LC}$ to 10 to better separate it from the pair creation zone, and increased μ to 2.5×10^4 to keep Φ_0 unchanged.

As we spin up the star, there is an initial burst of pair creation due to the vacuum initial condition and the induced $E_\parallel$ accelerating charges extracted from the surface. The system is able to form an almost FF configuration for a short time, then $E_\parallel$ gets screened inside the pair-creation zone, and the magnetosphere relaxes to a different state. After about 2 rotations of the star, $\rho \approx \rho_{\rm GJ}$ is sustained only at $r \lesssim 4$, and outside this zone the magnetosphere is close to the electrosphere solution (Figure 5). It stays in this state till the end of the simulation (about 8 rotations), with no pair creation.

In the final state, the magnetic field is everywhere similar to the dipole. The plasma

forms the negative "dome" and positive "torus" with a vacuum gap between them at $r \gtrsim 4$. The gap is outside the pair-creation zone and finds no way for plasma supply. The unscreened $E_\parallel$ in the gap creates a large potential drop along the magnetic field lines, which leads to faster rotation of the magnetosphere in the equatorial region at $r \sim 5 - 8$ (cf. Wada & Shibata 2011).

The magnetosphere is not completely dead at the end of the simulation. There is a weak negative current flowing out in the polar cap region, and a weak positive current leaking out from the tip of the "torus" region due to a strong $E_r \approx B$. At later times we expect the magnetosphere to evolve even closer to the electrosphere solution. The gap will tend to expand toward the null point $\rho_{\rm GJ} = 0$ on the star surface, into the zone where pair creation is possible. Then the discharge should reignite and prevent the inward expansion of the gap. The duration of our simulation is too short to see this late evolution; however, it is sufficiently long to show that type II rotators have a low level of activity most of the time.

Breaking the axisymmetry should initiate the diocotron instability (Philippov & Spitkovsky 2014); however it is unlikely to prevent the inner zone from filling with plasma and shutting down pair creation. Our simulations suggest that type II rotators cannot relax to the GJ state — it is unstable even with suppressed azimuthal perturbations; allowing the diocotron instability cannot make the GJ state an attractor for the system.

5. Discussion

Our first conclusion is that significant activity of the axisymmetric pulsar requires pair creation enabled at $r \sim R_{\rm LC}$ (called type I in this paper); this requires a sufficient optical depth to photon-photon collisions. If pair creation is limited to $r \ll R_{\rm LC}$ (type II), the return current is choked and the axisymmetric magnetosphere relaxes to the dome+torus state with suppressed electric currents and pair creation. Many observed pulsars are only capable of pair creation at $r \ll R_{\rm LC}$; we conclude that their activity and spindown should be a result of the misalignment of $\boldsymbol{\Omega}$ and $\boldsymbol{\mu}$. This conclusion supports the arguments of Michel (2004) and disagrees with the models of Goldreich & Julian (1969), Ruderman & Sutherland (1975), and Gruzinov (2013).

Type I axisymmetric rotators are active, as long as discharge voltage $\Phi_{\rm thr} < \Phi_0 = \mu\Omega^2/c^2$. Their spindown power is $L_{\rm sd} \approx \mu^2\Omega^4/c^3$ and their magnetic configuration is similar to the FF solution. Our numerical experiment shows, for the first time, how particle acceleration and $e^\pm$ discharge self-organize to maintain this configuration. The result is quite different from the previously discussed "trio" of gaps: polar-cap gap, slot gap, and outer

gap. Neither aligned nor anti-aligned rotators sustain pair creation in the polar cap outflow. Strong particle acceleration and pair creation occur in (and around) the return current sheet stretched along the boundary of the closed zone. The acceleration mechanism is different from the slot-gap models, which were developed for the opposite, polar-cap current. It is also different from the outer gap model where the null surface $\rho_{\rm GJ} = 0$ plays a key role. We find that the current sheet has $|\rho| \gg |\rho_{\rm GJ}|$, and its $E_\parallel$ is not controlled by the local value of $\rho_{\rm GJ}$.

Our numerical experiment confirms the phenomenological description of the gamma-ray source as an accelerator stretched along the boundary of the closed zone, which explains the observed pulse profiles of GeV emission (Dyks & Rudak 2003). The angular distribution of gamma-ray luminosity is determined by how $E_\parallel$ and $e^\pm$ discharge self-organize to sustain the magnetospheric configuration; the geometry by itself does not determine this distribution.

Besides producing copious $e^\pm$ pairs, type I rotators eject a significant flux of ions, $\dot{N}_i$. The anti-aligned rotator ejects $\dot{N}_i \approx I_{\rm GJ}/e$ from the polar cap, with low energies. The aligned rotator in our simulation ejects $\dot{N}_i \sim 0.1 I_{\rm GJ}/e$ along the current sheet, with much higher energies, which carries $\sim 5\%$ of the spindown power.

It remains to be seen which features of the axisymmetric magnetosphere will hold for inclined rotators. FF models provide guidance as they show where the current should flow. In contrast to the axisymmetric case, inclined rotators have $\alpha < 0$ and $\alpha > 1$ in the central region of the polar cap, which is required to activate $e^\pm$ discharge (Beloborodov 2008; Chen & Beloborodov 2013; Timokhin & Arons 2013). A current sheet with $|\alpha| \gg 1$ is expected to form along the boundary of the closed zone and produce gamma-rays similar to the mechanism seen in our simulations.

Our results show that key puzzles in pulsar physics can be solved using first-principle calculations, opening exciting opportunities for future modeling. This includes the global magnetic configuration, particle acceleration, pair multiplicity, and broad-band radiation, from curvature gamma-rays to coherent radio waves.

This work was supported by NASA grant NNX 13AI34G. We thank Benoît Cerutti, Andrei Gruzinov, Kyle Parfrey, and Anatoly Spitkovsky for helpful discussions.

REFERENCES

Arons, J. 1983, ApJ, 266, 215

Beloborodov, A. M. 2008, ApJ, 683, L41

Beloborodov, A. M., & Thompson, C. 2007, ApJ, 657, 967

Chen, A. Y., & Beloborodov, A. M. 2013, ApJ, 762, 76

Cheng, K. S., Ho, C., & Ruderman, M. 1986, ApJ, 300, 500

Contopoulos, I., Kazanas, D., & Fendt, C. 1999, ApJ, 511, 351

Dyks, J., & Rudak, B. 2003, ApJ, 598, 1201

Esirkepov, T. Zh. 2001, CoPhC, 135, 144

Goldreich, P., & Julian, W. H. 1969, ApJ, 157, 869

Gruzinov, A. 2013, arXiv e-print 1303.4094

Kalapotharakos, C., & Contopoulos, I. 2009, A&A, 496, 495

Krause-Polstorff, J., & Michel, F. C. 1985, MNRAS, 213, 43P

Jackson, E. A. 1976, ApJ, 206, 831

Michel, F. C. 2004, Advances in Space Research, 33, 542

Muslimov, A. G., & Harding, A. K. 2004, ApJ, 606, 1143

Parfrey, K., Beloborodov, A. M., & Hui, L. 2012, MNRAS, 423, 1416

Pétri, J., Heyvaerts, J., & Bonazzola, S. 2002, A&A, 387, 520

Philippov, A. A., & Spitkovsky, A. 2014, ApJ, 785, L33

Ruderman, M. A., & Sutherland, P. G. 1975, ApJ, 196, 51

Shibata, S. 1985, Ap&SS, 108, 337

Spitkovsky, A. 2006, ApJ, 648, L51

Spitkovsky, A., & Arons, J. 2002, Neutron Stars in Supernova Remnants, 271, 81

Sturrock, P. A. 1971, ApJ, 164, 529

Timokhin, A. N. 2006, MNRAS, 368, 1055

Timokhin, A. N., & Arons, J. 2013, MNRAS, 429, 20

Wada, T., & Shibata, S. 2011, MNRAS, 418, 612

Yuki, S., & Shibata, S. 2012, PASJ, 64, 43

This preprint was prepared with the AAS LaTeX macros v5.2.